IEEE Access
Multidisciplinary | Rapid Review | Open Access Journal

Received August 4, 2018, accepted September 24, 2018, date of publication October 1, 2018, date of current version October 19, 2018.

Digital Object Identifier 10.1109/ACCESS.2018.2872529

Formation Control of Multiple Unmanned Aerial Vehicles by Event-Triggered Distributed Model Predictive Control

ZHIHAO CAI[1], HUI ZHOU[1], JIANG ZHAO[1], KUN WU[2], AND YINGXUN WANG[1]
[1]School of Automation Science and Electrical Engineering, Beihang University, Beijing 100191, China
[2]Flying College, Beihang University, Beijing 100191, China

Corresponding author: Jiang Zhao (jzhao@buaa.edu.cn)

This work was supported in part by the National Natural Science Foundation of China under Grant 61803009, in part by the Fundamental Research Funds for the Central Universities under Grant YWF-18-BJ-Y-190, and in part by the Aeronautical Science Foundation of China under Grant 20175851032.

ABSTRACT This paper proposes an event-triggered model predictive control (MPC) scheme for the formation control of multiple unmanned aerial vehicles (UAVs). A distributed MPC framework is designed in which each UAV only shares the information with its neighbors, and the obtained local finite-horizon optimal control problem (FHOCP) can be solved by a swarm intelligent optimization algorithm. An event-triggered mechanism is proposed to reduce the computational burden for the distributed MPC scheme, which takes into consideration the predictive state errors as well as the convergence of cost function. Furthermore, a safe-distance-based strategy for no-fly zone avoidance is developed and integrated into the local cost function for each FHOCP. Numerical simulations show that the proposed event-triggered distributed MPC is more computationally efficient to achieve formation control of multiple UAVs in comparison with the traditional distributed MPC method.

INDEX TERMS Unmanned aerial vehicles (UAVs), formation control, distributed algorithms, predictive control, event-triggered, no-fly zone avoidance.

I. INTRODUCTION

Unmanned Aerial Vehicles (UAVs) have gained an increasing interest in several important areas, such as complex tasks including surveillance, agriculture irrigation, forestry fire prevention, cargo transportation, and coordinated rescue missions in the presence of disturbances, failures, and uncertainties [1]–[4]. A swarm of UAVs could be a more effective system than a single vehicle, and the formation control is a critical step of attempting to the cooperation among UAVs. Extensive research has been conducted on the formation control of UAV swarm to fulfill cooperative missions.

The common approaches of formation control for multiple UAVs include consensus theory, leader-follower strategy, behavior-based method, virtual structure approach, differential game, finite-time control theory, etc. In [5], a novel formation control algorithm suitable for both leaders and followers is designed, in which leaders are implicitly integrated into the swarm and can be influenced by navigational feedback from their flock mates. A method which based on the common Lyapunov functional method and algebraic Riccati equation technique to design the protocol for formation control is presented in [6]. Based on homing pigeon hierarchical strategies, a distributed formation control framework is proposed in [7], which combines the advantages of velocity correlation, leader-follower interaction and hierarchical leadership network observed in pigeon flock with altitude consensus control algorithm used in UAV formation control. An approach of hybrid supervisory control for a two-dimensional leader-follower formation scenario is presented in [8], which is able to capture internal relations between the path planner and the decision-making unit of multiple UAVs. In [9], a novel switching approach based on the binary-tree network is developed to realize the transformations between the V-shape and the complete binary tree shape (CBT-shape) topologies. The formation control problem is formulated and solved as a differential game problem. In [10], a novel strategy design method of open-loop Nash is proposed for each UAV to implement in a fully distributed manner through

estimating its terminal state. Based on the finite-time control theory, a distributed formation control protocol is proposed in [11]. Through the design of the control law, the multi-UAV systems is able to achieve the desired formation in a limited time. And according to the requirements of formation control, the formation configurations can be specified in advance.

The model predictive control (MPC) approach also shows good performance in UAV formation control. In [12], a controller of collision-free UAV formation flight is designed for the framework of MPC. Based on MPC scheme, an online three-dimension path-planning method is proposed for multiple UAVs in the partially known task environment [13]. In addition, the linear and nonlinear control policies are applied as a high-level controller for multiple UAVs to surround the expected target in simulations and real-time quadrotor experiments [14]. However, most MPC schemes for cooperative flight control, such as those in [15] and [16], are designed on the basis of time-triggered mechanism. The control actions are periodically executed even if the systems have achieved desired control performance. Therefore, event-triggered mechanism is integrated into the MPC scheme to reduce computational load or communication consumption [17]–[20]. Based on the above prototype work, this paper proposes a distributed MPC scheme for UAV formation control with event-triggered mechanism [21], which can enable the FHOPC to be solved asynchronously and reduce the computational burden.

The contribution of the paper is described as follows: 1) the distributed MPC scheme is developed for UAV formation control, each of which only shares information with its neighbors and solves its own local optimization problem; 2) an event-triggered mechanism is proposed for the distributed MPC scheme considering the predictive state errors and the convergence of cost function which can reduce the computational burden; 3) the safe-distance-based strategy for no-fly zone avoidance is developed and integrated into the local cost function for formation control.

The paper is organized as follows. Section 2 presents the formation model, constrained PSO solver, and nonlinear MPC. In Section 3, the design of the distributed MPC scheme based on event-triggered mechanism is proposed in detail. The numerical simulations in Section 4 demonstrate the effectiveness of the proposed distributed MPC scheme. Finally, concluding remarks are presented in Section 5.

II. PRELIMINARIES

A. FORMATION MODEL

Suppose that N UAVs are expected to achieve formation keeping and track a reference trajectory according to various tasks. Assuming that each UAV is considered as the mass point in the two-dimensional plane, the motion of UAV formation can be depicted in Fig. 1.

Herein, each member in the UAV formation is assumed identical. The motion states of the UAV i defined by

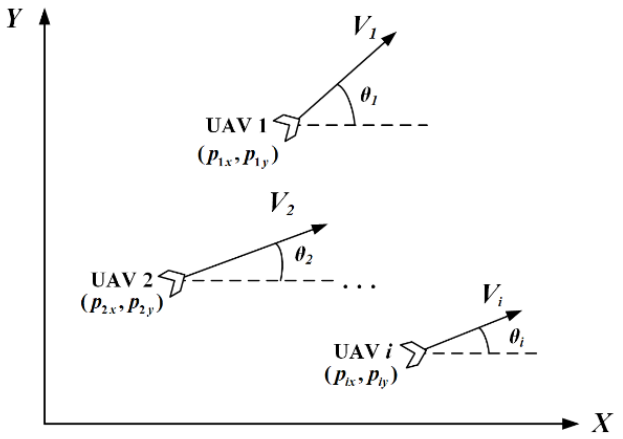

FIGURE 1. The motion of UAV formation.

$z_i = [p_{ix}, p_{iy}, \theta_i, v_i]^T$ can be described by

$$\begin{cases} \dot{p}_{ix} = v_i \cos\theta_i \\ \dot{p}_{iy} = v_i \sin\theta_i \\ \dot{\theta}_i = \omega_i \\ \dot{v}_i = a_i, \end{cases} \quad i = 1, 2, \ldots, N \tag{1}$$

where v_i and θ_i are the linear velocity and yaw angle of each UAV. a_i and ω_i are the accelerated velocity and angular velocity, respectively. $p_i = [p_{ix}, p_{iy}]^T$ consists of the abscissa value p_{ix} and ordinate value p_{iy}.

B. NONLINEAR MPC

Considering the nonlinear MPC problem, the UAV dynamics (1) can be written as the following equivalent form

$$\dot{z}(t) = f(z(t), u(t)), \quad t \geq t_0,\ z(0) = z_0 \tag{2}$$

where $z(t) \in \mathcal{R}^n$ is the system state trajectory, and $u(t) \in \mathcal{R}^m$ is the system control trajectory. Then, define the constant prediction horizon and the constant control update period as $T_\mathrm{p} \in (0, \infty)$ and $\delta \in (0, T_\mathrm{p}]$, respectively. The common receding horizon update times are described as $t_c = t_0 + \delta c$, $c \in \{0, 1, 2, \ldots\}$. At each time instant t_c, the problem of MPC can be determined by the following finite horizon optimal control problem (FHOCP).

Problem 1: For each member $i \in \{1, 2, \ldots, N_\mathrm{m}\}$ and at the update time instant $t_c = t_0 + \delta c$, $c \in \{0, 1, 2, \ldots\}$: Given $z(t_c)$, and then, find

$$u^*(s; t_c) = \arg\min_{u(s;t_c)} J(z(s; t_c), u(s; t_c)) \tag{3}$$

$$J(z(s; t_c), u(s; t_c)) = \int_{t_c}^{t_c+T_\mathrm{p}} F(z(s; t_c), u(s; t_c))\, ds + \Phi\left(z\left(t_c + T_\mathrm{p}; t_c\right)\right) \tag{4}$$

$$\text{subject to } \dot{z}(t) = f(z(t), u(t)), \quad t \geq t_0,\ z(0) = z_0 \tag{5}$$

$$z(s; t_c) \in Z \tag{6}$$
$$u(s; t_c) \in Y \tag{7}$$

where $s \in [t_c, t_c + T_p]$ is the prediction horizon. $z(s; t_c)$ and $u(s; t_c)$ are the predicted state trajectory and predicted control trajectory, respectively. $u^*(s; t_c)$ is the optimal control trajectory. Z and Y are constraints of state and control input. J is the integrated cost function which includes a running function F and a terminal state penalty function Φ.

C. CONSTRAINED PSO SOLVER

In this paper, the basic version of the global particle swarm algorithm is used because it is well suitable for solving the optimal solution of trajectory optimization problems. It is assumed that $\{x_1, x_2, \ldots, x_n\}$ are the n unknown parameters that have their own limitations as follow

$$x_i \in [la_i, lb_i] \quad (i = 1, 2, \ldots, n) \tag{8}$$

where la_i and lb_i are the lower and upper limitations of the i-th unknown parameter, respectively. A swarm of M particles represents the population in the PSO. Then, each particle m is associated with a position vector $x(m)$ and a velocity vector $v(m)$ as

$$x(m) = [x_1(m), x_2(m), \ldots, x_n(m)]^{\mathrm{T}} \quad (m = 1, 2, \ldots, M) \tag{9}$$

$$v(m) = [v_1(m), v_2(m), \ldots, v_n(m)]^{\mathrm{T}} \quad (m = 1, 2, \ldots, M) \tag{10}$$

where the terms $x(m)$ and $v(m)$ are referred to the search space of the n unknown parameters. The elements of the two vectors are represented by $x_i(m)$ and $v_i(m)$ $(i = 1, 2, \ldots, n)$. Based on the limitations of the n unknown parameters, the related position and velocity components are limited to

$$\begin{cases} la_i \le x_i(m) \le lb_i \\ |v_i(m)| \le |la_i - lb_i| \end{cases} \quad (i = 1, 2, \ldots, n; m = 1, 2, \ldots, M) \tag{11}$$

The particle which is described by the terms $x(m)$ and $v(m)$ represents a possible solution to the optimization problem and leads to a specific value of the objective function. Assume that the PSO algorithm terminates at the maximum number of the iterations NIT. In a generic iteration j $(j = 1, 2, \ldots, NIT)$, the fitness function is evaluated with the particle m. The best position $pbest^{(j)}(m)$ ever visited by the particle m is determined. Then, the global best position $gbest^{(j)}(m)$ ever visited is determined by the swarm, so that the update of the velocity vector for each particle m can be expressed as

$$v^{(j+1)}(m) = wv^{(j)}(m) + c_1 r_1(0, 1)\left(\mathbf{p}_{\mathrm{best}}^{(j)}(m) - x^{(j)}(m)\right) + c_2 r_2(0, 1)\left(\mathbf{g}_{\mathrm{best}}^{(j)}(m) - x^{(j)}(m)\right) \quad (m = 1, 2, \ldots, \mathrm{M}) \tag{12}$$

where $x^{(j)}(m)$ and $v^{(j)}(m)$ are the position vector and velocity vector in each iteration, respectively; the inertial weight is expressed by w; the influences of the cognitive and social components are expressed by c_1 and c_2, respectively; r_1 (0, 1) and r_2 (0, 1) are independent random numbers between 0 and 1. At this rate, the update of the position vector for each particle m is described as

$$x^{(j+1)}(m) = x^{(j)}(m) + v^{(j)}(m) \quad (m = 1, 2, \ldots, M) \tag{13}$$

For the equality constraints, the most typical solution is to add a penalty term to the fitness function, which reflects the sum of the absolute values defined from the equality constraints:

$$J' = J + \sum_{p=1}^{m} \zeta_p \left| d_p(x) \right| \tag{14}$$

where $\zeta_p \ge 0\,(p = 1, 2, \ldots, m)$ is the weight factor; $d_p(x)$ $(p = 1, 2, \ldots, m)$ represents the m quality constraints associated with the n unknown parameters. For inequality constraints, a simple solution is to set the fitness function to an infinite value $\left(J^{(j)}(m) = \infty\right)$ if the particle m violates one of the inequality constraints. In general, the related velocity is also set to zero $\left(v^{(j)}(m) = 0\right)$ so that the velocity update is only affected by the social and cognitive components.

III. EVENT-TRIGGERED DISTRIBUTED MPC FOR FORMATION CONTROL

A safe-distance-based strategy for no-fly zone avoidance is developed and integrated into the distributed MPC scheme. An event-triggered mechanism is proposed to reduce the computational burden of the distributed MPC scheme.

A. DISTRIBUTED MPC SCHEME

The decoupled time-invariant nonlinear dynamics for UAV i can be written in the equivalent form as

$$\dot{z}_i(t) = f_i(z_i(t), u_i(t)), \quad t \ge t_0 \tag{15}$$

and then, $z = (z_1, z_2, \ldots, z_N)$, $u = (u_1, u_2, \ldots, u_N)$ and $f(z, u) = (f_1(z_1, u_1), f_2(z_2, u_2), \ldots, f_N(z_N, u_N))$ represent the concatenated vectors in the system (2).

For the traditional MPC framework in **Problem 1**, the state of each UAV is typically coupled in the integrated cost function to achieve the UAV formation control. The common components in (4) can be expressed as

$$F(z(t), u(t)) = \alpha \sum_{(i,j)\in\mathcal{A}} \left\| p_i(t) - p_j(t) - p_{ij}^d(t) \right\|^2 + \beta \left\| \frac{1}{N} \sum_{i\in\varsigma} p_i(t) - p_O^d(t) \right\|^2 \tag{16}$$

where $p_{ij}^d(t)$ represents the desired relative position between each UAV. $p_O^d(t)$ represents the reference trajectory. $\varsigma = \{1, 2, \ldots, N\}$ represents the set of UAVs. The set of the pair-wise neighbors in the multi-UAV network is expressed by $\mathcal{A}$. Assume that if $(i, j) \in \mathcal{A}$, then define $(j, i) \notin \mathcal{A}$ and $(i, i) \notin \mathcal{A}$ for UAV $i \in \varsigma$. Both the term α and term β are

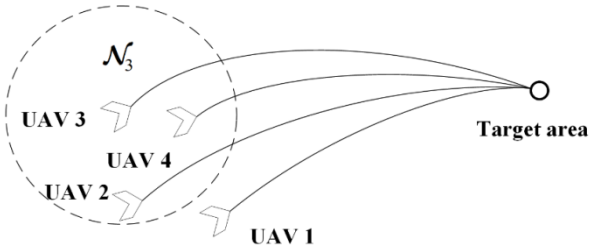

FIGURE 2. Example of the communication limitation in the multi-UAV network.

the weighting constants. The symbol $\|\cdot\|$ denotes any vector norm in $\mathcal{R}^n$.

The main advantage of the traditional MPC framework is that the cost function with (16) is designed, and the state trajectories and control trajectories of all UAVs are considered. It can fully reflect the motion of the multi-UAV network. However, the requirement of computation load is typically high and the approach would be out of work if some UAV is only able to obtain the effective information from its neighbors. Fig. 2 illustrates an example of communication limitation in the multi-UAV network that UAV i can only communicate with its neighbors in the set $\mathcal{N}_i$. UAV i can also obtain the estimated information of non-neighbors indirectly from its neighbors. The total number of UAVs in the set $\mathcal{N}_i$ is N_i.

As shown in Fig. 3, the distributed MPC framework is proposed for the multi-UAV network. At each update instant, the control inputs of the group of UAVs are first initialized by using the previous predicted optimal control trajectories. Then, each UAV receives the estimated control trajectories from its neighbors. The estimated state trajectories are computed based on the control trajectories of the neighbors in the last period and the control trajectories of the non-neighbors in the last two periods, in which the information from non-neighbors is indirectly transmitted from neighbors. Based on the estimated state trajectories and estimated control trajectories from neighbors, each UAV evaluates the distributed cost function of its own and finds the optimal predicted control trajectory over the current prediction horizon. Finally, the optimal control trajectories over the first control update period is implemented to update the states of each UAV.

In order to describe the distributed MPC scheme, we first define that the neighbors of each UAV $i \in \varsigma$ with the control vectors state vectors $z_{-i}(t) = \{z_j(t)\}, j \in \mathcal{N}_i$ and $u_{-i}(t) = \{u_j(t)\}, j \in \mathcal{N}_i$, respectively. The decoupled nonlinear dynamics of the neighbors of UAV i can be expressed as

$$\dot{z}_{-i}(t) = f_{-i}(z_{-i}(t), u_{-i}(t)), \quad t \geq t_0 \tag{17}$$

hen, the following symbols are defined to distinguish the different types of the state trajectory and control trajectory for each UAV i at current instant t_c

1. $u_i^p(s; t_c)$, $z_i^p(s; t_c)$: the predicted control trajectory and predicted state trajectory;

2. $u_i^*(s; t_c)$, $z_i^*(s; t_c)$: the optimal predicted control trajectory and optimal predicted state trajectory;

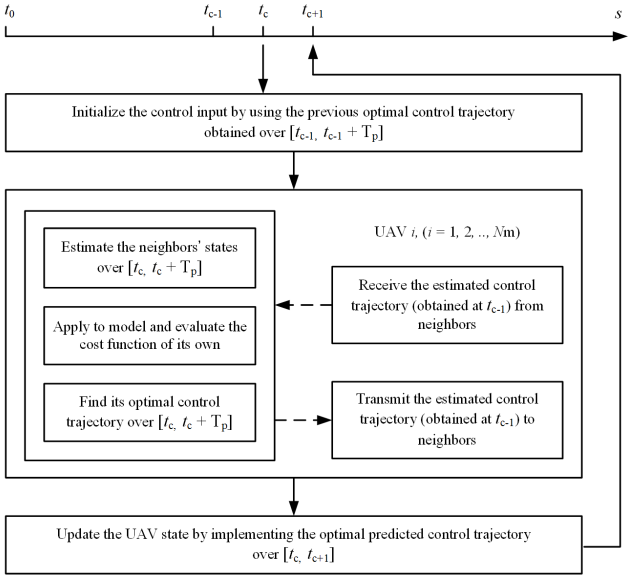

FIGURE 3. Framework of the distributed MPC scheme.

3. $\hat{u}_i(s; t_c)$, $\hat{z}_i(s; t_c)$: the estimated control trajectory and estimated state trajectory.

where $s \in [t_c, t_c + T_p]$ is the given prediction horizon. Consistent with $u_{-i}(t)$ and $z_{-i}(t)$, the estimated control trajectory and estimated state trajectory for the neighbors of each UAVi are denoted as $\hat{u}_{-i}(s; t_c)$ and $\hat{z}_{-i}(s; t_c)$, respectively.

The estimated control trajectory $\hat{u}_{-i}(s; t_c)$ and the estimated state trajectory $\hat{z}_{-i}(s; t_c)$ over the prediction horizon $s \in [t_c, t_c + T_p]$ will be determined at each update instant t_c. As shown in Fig. 3, it is typically an iterative process in the proposed distributed MPC scheme by continuously updating the time constant $t_c = t_0 + \delta c$, $c \in \{0, 1, 2, \ldots\}$.

In each iterative process, the estimated control trajectory of its neighbor over the prediction horizon $s \in [t_c, t_c + T_p]$ is described according to the above definition $u_{-i}(t) = \{u_j(t)\}, j \in \mathcal{N}_i$. Specifically, the estimated control trajectory $\hat{u}_{-i}(s; t_c)$ can be expressed as

$$\hat{u}_{-i}(s; t_c) = \left\{\hat{u}_j(s; t_c)\right\}, \quad j \in \mathcal{N}_i \tag{18}$$

where the estimated control trajectory $\hat{u}_j(s; t_c)$ consists of two separate parts over the prediction horizon $s \in [t_c, t_c + T_p]$. As shown in Fig. 4, the first part of the estimated control trajectory $\hat{u}_j(s; t_c)$ inherits the previous optimal control trajectory $u_j^*(s; t_{c-1})$ over the prediction horizon $s \in [t_c, t_{c-1} + T_p)$. The second part of the estimated trajectory $\hat{u}_j(s; t_c)$ over the prediction horizon $s \in [t_{c-1} + T, t_c + T_p]$ is derived from the previous optimal control trajectory $u_j^*(s; t_{c-1})$ at the time instant $s = t_{c-1} + T_p$. Specifically, the estimated control trajectory $\hat{u}_j(s; t_c)$ can be formulated as

$$\hat{u}_j(s; t_c) = \begin{cases} u_j^*(s; t_{c-1}), & s \in \left[t_c, t_{c-1} + T_p\right) \\ u_j^*\left(t_{c-1} + T_p; t_{c-1}\right), & s \in \left[t_{c-1} + T_p, t_c + T_p\right] \end{cases} \tag{19}$$

By using (18) and (19), the estimated control trajectory of the neighboring UAV, $\hat{u}_{-i}(s; t_c)$, is obtained. Then, the

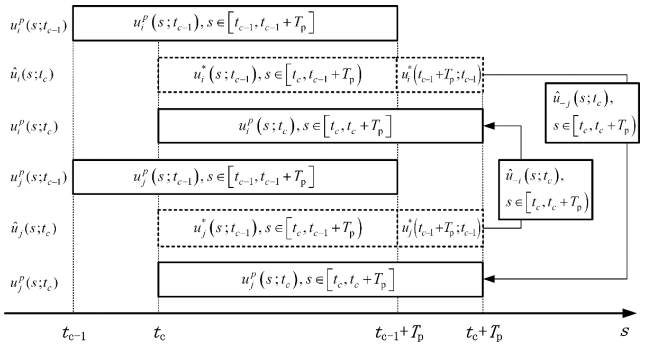

FIGURE 4. Generation of the estimated control and state trajectories.

relevant estimated state trajectories $\hat{z}_{-i}(s;t_c)$ can be also obtained according to the dynamics (17).

Define $g \notin \mathcal{N}_i$, and the estimated control trajectories of the non-neighbors in the last two period is transmitted by its neighbor. The estimated control trajectory $\hat{u}_g(s;t_c)$ consists of two parts over the prediction horizon $s \in [t_c, t_c+T_p]$. The first part of the estimated control trajectory $\hat{u}_g(s;t_c)$ inherits the previous optimal control trajectory $u_g^*(s;t_{c-1})$ over the prediction horizon $s \in [t_c, t_{c-2}+T_p)$. The second part of the estimated trajectory $\hat{u}_g(s;t_c)$ over the prediction horizon $s \in [t_{c-2}+T, t_c+T_p]$ is derived from the previous optimal control trajectory $u_g^*(s;t_{c-2})$ at the time instant $s = t_{c-2}+T_p$. The estimated control trajectory $\hat{u}_g(s;t_c)$ can be formulated in the form of

$$\hat{u}_g(s;t_c) = \begin{cases} u_g^*(s;t_{c-2}), & s \in [t_c, t_{c-2}+T_p) \\ u_g^*(t_{c-2}+T_p;t_{c-2}), & s \in [t_{c-2}+T_p, t_c+T_p] \end{cases} \tag{20}$$

The estimated state trajectory is used to predict the state of each UAV in the next control period by imposing the same control command in the last control horizon. Since the computation frequency of FHOCP can be reduced to a certain extent by including the event-triggered mechanism, the control command imputed to each agent will not change frequently. Thus, by imposing the control command in the last control period, the predictive state error resulted by the assumed state trajectory may have little impact on the convergence of the FHOCP.

According to the formulation of the estimated control and state trajectories, the distributed cost function of each UAV $i \in \varsigma$ is expressed as

$$\begin{aligned} &F_i\left(z_i^p(s;t_c), \hat{z}_{-i}(s;t_c), u_i^p(s;t_c)\right) \\ &= \alpha \sum_{j\in\mathcal{N}_i} \left\| p_i^p(s;t_c) - \hat{p}_j(s;t_c) - p_{ij}^d(s;t_c) \right\|^2 \\ &\quad + \beta \left\| \frac{1}{N}\left(p_i^p(s;t_c) + \sum_{j\in\mathcal{N}_i} \hat{p}_j(s;t_c) + \sum_{g\notin\mathcal{N}_i} \hat{p}_g(s;t_c) \right) \right. \\ &\quad \left. - p_O^d(s;t_c) \right\|^2 \end{aligned} \tag{21}$$

where the nonlinear MPC problem at each time instant t_c can be described by the following distributed FHOCP.

Problem 2: For each member $i \in \{1, 2, \ldots, N\}$ and at the update time $t_c = t_0 + \delta c$, $c \in \{0, 1, 2, \ldots\}$: Given $z_i(t_c)$, $z_{-i}(t_c)$, $\hat{u}_i(s;t_c)$, $\hat{u}_{-i}(s;t_c)$, $s \in [t_c, t_c+T_p]$, and then, find

$$u_i^*(s;t_c) = \arg\min_{u_i(s;t_c)} J_i(z_i(s;t_c), z_{-i}(s;t_c), u_i(s;t_c)) \tag{22}$$

$$J_i\left(z_i^p(s;t_c), \hat{z}_{-i}(s;t_c), u_i^p(s;t_c)\right) = \int_{t_c}^{t_c+T_p} F_i\left(z_i^p(s;t_c), \hat{z}_{-i}(s;t_c), u_i^p(s;t_c)\right) ds \tag{23}$$

$$\text{subject to } \dot{z}_i^p(s;t_c) = f_i\left(z_i^p(s;t_c), u_i^p(s;t_c)\right) \tag{24}$$

$$\dot{\hat{z}}_{-i}(s;t_c) = f_{-i}\left(\hat{z}_{-i}(s;t_c), \hat{u}_{-i}(s;t_c)\right) \tag{25}$$

$$z_i^p(s;t_c), \quad \hat{z}_{-i}(s;t_c) \in Z \tag{26}$$

$$u_i^p(s;t_c), \quad \hat{u}_{-i}(s;t_c) \in Y \tag{27}$$

where $s \in [t_c, t_c+T_p]$ is the prediction horizon. J_i is the distributed cost function of each UAV i including a running function F_i. The optimal control trajectory of each UAV $i \in \varsigma$ is expressed as $u_i^*(s;t_c)$.The pseudo-code of the distributed MPC scheme is listed in **Algorithm 1**.

In this paper, the problem of UAV formation control is transformed into a series of local FHOCP in the distributed MPC framework. Problems 1 and 2 are the traditional and distributed MPC problems, in which the control input of each UAV is obtained by solving the FHOCP. The PSO algorithm is selected as a convenient tool to solve Problems 1 and 2. The PSO algorithm can be used for both on-line and off-line computation. The convergence time of the proposed MPC scheme is mainly determined by the population size and iteration number of the PSO algorithm. Large population size and iteration number will lead to satisfied optimal results, and however, may increase the convergence time of the PSO solver. Therefore, a compromise selection of population size and iteration number is used in this paper to ensure both the optimal results and convergence time.

B. NO-FLY ZONE CONSTRAINT

With the increasing demand for adaptive guidance and control approaches, the threat avoidance and geopolitical restriction have been considered for the UAVs [22], unmanned surface vehicles [23], autonomous underwater vehicles [24], and mobile robots [25]. In complex environments, the no-fly zone constraint is also essential for the development of the guidance and control systems. For this reason, recent studies have focused on the design of reference routes [26] and guidance laws [27] considering the no-fly zone constraint. In order to improve the performance of multi-UAV network in detecting the target and penetrating the defense system, the no-fly zone constraint is discussed in this section, which enhances the UAV formation control method.

Fig. 5 shows the geometry of the UAV with no-fly zone constraint. Herein, the circular no-fly zone is used because

Algorithm 1 Pseudo-Code of the Distributed MPC Scheme for Each UAV $i \in \{1, 2, \ldots, N\}$

1: // Initialization: at time t_0
2: Set the parameters of the algorithm: T_p, δ
3: Initialize the state inputs: $z_i(t_0)$, $z_{-i}(t_0)$
4: Set $\hat{u}_i(s; t_0) = 0, \hat{u}_{-i}(s; t_0) = 0, s \in [t_0, t_0 + T_\mathrm{p}]$ and solve **Problem** 2 for UAV i, yielding the optimal predicted control trajectory $u_i^*(s; t_0)$, $s \in [t_0, t_0 + T_\mathrm{p}]$
5: Apply the first control input $u_i^*(s; t_0)$, $s \in [t_0, t_1)$
6: **// Main loop:** at any time $t_c = t_0 + \delta c$, $c = \{1, 2, \ldots\}$
7: Measure the current state $z_i(t_c)$
8: Transmit $\hat{u}_i(s; t_{c-1})$, $s \in [t_c, t_{c-1} + T_\mathrm{p}]$ to its every neighbor
9: Receive $\hat{u}_j(s; t_{c-1})$, $s \in [t_c, t_{c-1} + T_\mathrm{p}]$ from its every neighbor j, and compute the estimated control and state trajectories $\hat{u}_{-i}(s; t_c)$, $\hat{z}_{-i}(s; t_c)$, $s \in [t_c, t_c + T_\mathrm{p}]$
10: Solve **Problem 2** for UAV i, yielding $u_i^*(s; t_c)$, $s \in [t_c, t_c + T_\mathrm{p}]$
11: Apply the first control input $u_i^*(s; t_c)$, $s \in [t_c, t_{c+1})$
12: **// Results**
13: Find the optimal control sequences and generate the complete trajectory
14: Validate the trajectory constraints and terminal conditions

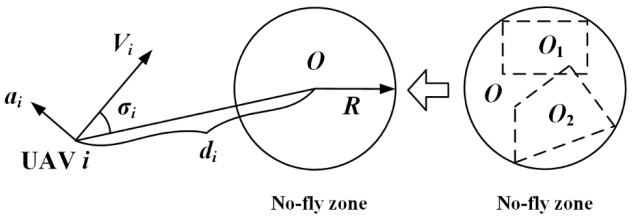

FIGURE 5. Geometry on the UAV with no-fly zone constraint.

any irregular no-fly zone can be simply replaced by it. The term R indicates the radius of the no-fly zone and d_i is the distance between the no-fly zone and UAV i. The angle $\sigma_i \in (-\pi, +\pi)$ is defined in the line-of-sight frame with respect to the center of the no-fly zone. It can be found that the no-fly zone constraint will possibly be violated as $d_i \to R$ and $|\alpha_i| \to 0$, whereas some larger d_i or $|\alpha_i|$ may protect the UAV against penetrating the no-fly zone.

In the paper, the term d_{safe} is used to describe the safe distance between each UAV and the center of the no-fly zone. The different cases of the UAV related to the no-fly zone are illustrated in Fig. 6. In order to meet the constraint of no-fly zone, as described above, the basic rule is to prevent every UAV from approaching and pointing to the center of the no-fly zone. Therefore, the terms d_i or $|\alpha_i|$ is employed to design the switching conditions under which the members in the multi-UAV network must react immediately. As shown in Fig. 6, it is considered that the no-fly zone constraint will be included in the optimization problem when any UAV i approaches within the unsafe distance $(i.e.\ d_i < d_{safe})$ and towards near the center of the no-fly zone $(i.e.\ |\alpha_i| < p/2)$.

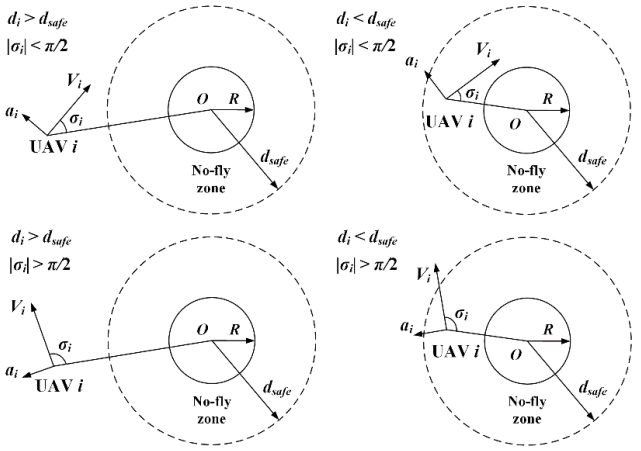

FIGURE 6. Different cases of the UAV in relation to the no-fly zone.

In other words, only when both two conditions above are met, the UAV will begin to adjust its acceleration command to avoid the no-fly zone.

Thus, a penalty term can be added to the distributed cost function to solve the problem of no-fly zone constraint. The cost function for each UAV i can be expressed as

$$\tilde{J}_i = J_i + \mu \frac{D(d_i, \sigma_i) \cos \sigma_i}{\|d_i\|^2} \tag{28}$$

where μ is the weighting constant. The term $D(d_i, \sigma_i)$ determines when the penalty term should be included in the cost function. The detailed form can be expressed as

$$D(d_i, \sigma_i) = \begin{cases} 1, & d_i < d_{safe} \text{ and } |\sigma_i| < \pi/2 \\ 0, & d_i \geq d_{safe} \text{ or } |\sigma_i| \geq \pi/2 \end{cases} \tag{29}$$

The terms d_i and σ_i are the relative distance and angle at current time which vary with control inputs u_i. Indeed, the penalty term added will be switched between 0 and a real number, which determines whether the penalty term for no-fly zone avoidance should be included in the cost function. In other words, during no-fly zone avoidance, equations (28) and (29) have an impact on threat avoidance by including the penalty term. The on-line computation of the proposed MPC scheme is mainly determined by the population size and iteration number of PSO algorithm. Large population size and iteration number will lead to satisfied optimal results, and however, may increase the convergence time of the PSO solver. Therefore, a compromise selection of population size and iteration number is used in this paper to ensure both the optimal results and convergence time.

C. EVENT-TRIGGERED MECHANISM

To reduce the computational burden for each UAV, an event-triggered mechanism is proposed to improve the performance of the distributed MPC scheme. The FHOCP will be solved when the event-triggered condition is satisfied. Suppose that the FHOCP is solved at t_k, the optimal predicted control trajectory $u_i^*(s; t_k)$ and the corresponding optimal

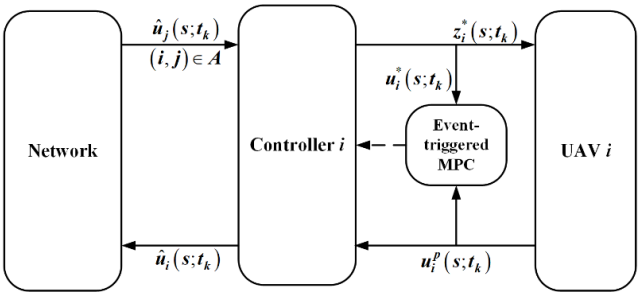

FIGURE 7. The framework of the distributed MPC scheme with event-triggered mechanism.

predicted state trajectory $z_i^*(s;t_k)$ for $s\in[t_k, t_k+T_p]$ can be obtained. Then, the next event-triggered instant t_{k+1} to solve the FHOCP is determined by the following event-triggered condition

$$E: if\ g_i(z(t),u(t))\geq 0,\quad then\ u(t_c)\leftarrow u^*(t_c|t_c) \tag{30}$$

which takes into consideration the no-fly zone constraint, saturation level of predictive control inputs, the predictive distance error between each UAV, the predictive distance error between the formation center and reference trajectory, the convergence of predictive cost function, the prediction horizon constraint, etc. Fig. 7 shows the framework of the distributed MPC scheme with event-triggered mechanism.

First, the no-fly zone constraint should be considered to design the event-triggered condition. When the predictive distance between UAV i and the center of no-fly zone exceeds the safe distance, the FHOCP should be solved. Thus, the event-triggered condition (30) can be replaced by

$$g_i(z(t),u(t)) = \Delta d_i(t) = d_{safe} - d_i^p(t) \tag{31}$$

where $d_i^p(t)$ is the predictive distance between UAV i and the center of no-fly zone. The corresponding event-triggered condition can be expressed as

$$E_1:\ if\ \Delta d_i(t_c) = d_{safe} - d_i^p(t_c)\geq 0,\quad then\ u(t_c)\leftarrow u^*(t_c|t_c) \tag{32}$$

Then, the saturation level of predictive control inputs should also be included in the design the event-triggered condition. When the predictive control inputs exceed the desired threshold, the FHOCP should be solved. The event-triggered condition (30) can be replaced by

$$g_i(z(t),u(t)) = \Delta u_i(t) = u_i^p(t) - \eta u_{\max},\quad u_{\max} = [a_{\max},\omega_{\max}]^T \tag{33}$$

where $\eta\in[0,1]$ indicates the saturation level of control inputs. The corresponding event-triggered condition can be expressed as

$$E_2:\ if\ \Delta u_i(t_c) = u_i(t_c) - \eta * u_{\max}\geq 0,\quad then\ u(t_c)\leftarrow u^*(t_c|t_c) \tag{34}$$

One of the key factors to determine when to solve the FHOCP is the predictive distance error between each UAV. If the predictive distances between each UAV are far from the desired values, the FHOCP should be solved. The event-triggered condition (30) can be replaced by

$$g_i(z(t),u(t)) = \Delta p_{ij}(t) = \left\| p_i^p(t) - \hat{p}_j(t) - p_{ij}^d(t)\right\|^2 - \varepsilon_P \tag{35}$$

where ε_P is the threshold of the predictive distance error. The corresponding event-triggered condition can be expressed as

$$E_3: if\ \Delta p_{ij}(t_c) = \left\| p_i^p(t_c) - \hat{p}_j(t_c) - p_{ij}^d(t_c)\right\|^2 - \varepsilon_p\geq 0,\quad then\ u(t_c)\leftarrow u^*(t_c|t_c) \tag{36}$$

The FHOCP should be solved when the predictive distance between the formation center and reference trajectory exceeds the certain threshold. The event-triggered condition (30) can be replaced by

$$\begin{aligned} g_i(z(t),u(t)) &= \Delta p_O(t)\\ &= \left\| \frac{1}{N_i}\left(p_i^p(t) + \sum_{j\in N_i}\hat{p}_j(t)\right) - p_O^d(t)\right\|^2 - \varepsilon_O \end{aligned} \tag{37}$$

where ε_O is the threshold of the predictive distance between the formation center and reference trajectory. The corresponding event-triggered condition can be expressed as

$$E_4:\ if\ \Delta p_O(t_c) = \left\| \frac{1}{N_i}\left(p_i^p(t_c) + \sum_{j\in N_i}\hat{p}_j(t_c)\right) - p_O^d(t_c)\right\|^2 - \varepsilon_c\geq 0,\quad then\ u(t_c)\leftarrow u^*(t_c|t_c) \tag{38}$$

Another key factor to determine when to solve the FHOCP is the convergence of predictive cost function. The decrease of the predictive cost value for each UAV can lead to the decrease of the state error of formation. If the predictive cost value of each UAV increases, the FHOCP should be solved. The event-triggered condition (30) can be replaced by

$$g_i(z(t),u(t)) = \Delta J_i(t) = J_i^p(t) - J_i(t-\Delta t_k) \tag{39}$$

where $J_i^p(t)$ is the predictive cost value, $J_i(t_{\Delta k})$ is the cost value at $\Delta t_k = \Delta k * \delta$, $\Delta k\in\{1,2,\ldots\}$. The corresponding event-triggered condition can be expressed as

$$E_5:\ if\ \Delta J_i(t_c) = J_i^p(t_c) - J_i(t_c-\Delta t_k)\geq 0,\quad then\ u(t_c)\leftarrow u^*(t_c|t_c) \tag{40}$$

In addition, if the control inputs are used more than the prediction horizon T_p, the FHOCP should be solved. The corresponding event-triggered condition can be expressed as

$$E_6:\ if\ !E_1\ and\ !E_2\ and\ !E_3\ and\ !E_4\ and\ !E_5,\quad then\ \begin{cases} u(t_c)\leftarrow u^*(t_c|t_{c-1}), & t_c < t_k+T_p\\ u(t_c)\leftarrow u^*(t_c|t_c), & t_c = t_k+T_p \end{cases} \tag{41}$$

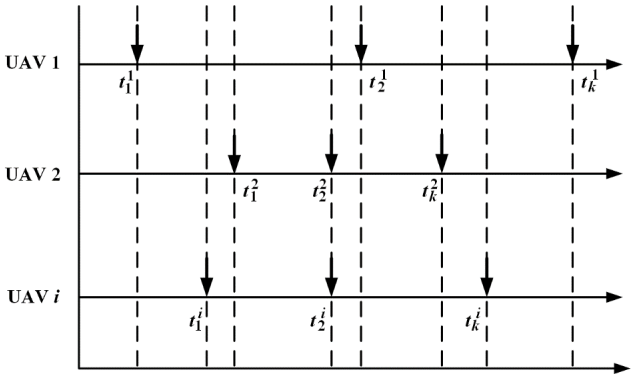

FIGURE 8. The event-triggered instants of each UAV.

It is assumed that the previous event-triggered instant of UAV i is t_k^i, the next event-triggered instant t_{k+1}^i can be expressed as

$$t_{k+1}^i = \min\left\{\bar{t}_{k+1}^i, t_k^i + T_p\right\} \tag{42}$$

where $\bar{t}_{k+1}^i > t_k^i$ is the event-triggered instant of the UAV i when the one of event-triggered conditions is satisfied. As shown in Fig. 8, the asynchronous event-triggered instants of each UAV can be expressed as $0 < t_1^i < \cdots < t_k^i < t_{k+1}^i$. The flow chart of the event-triggered mechanism is shown in Fig. 9.

Based on the above event-triggered mechanism, the pseudo-code of the distributed MPC scheme for multiple UAVs is listed in **Algorithm 2**.

IV. NUMERICAL SIMULATIONS

In this section, a simulation scenario of formation control of three UAVs is performed to demonstrate the effectiveness of the proposed distributed MPC scheme based on event-triggered mechanism. A simple communication topology is selected for three UAVs. Each member can obtain the information from the neighbors, i.e. $\mathcal{N}_1 = \{2\}$, $\mathcal{N}_2 = \{1, 3\}$ and $\mathcal{N}_3 = \{2\}$. Communication topology in the multi-UAV network.is shown in Fig. 10. The desired distances between each UAV are set to $p_{12} = -p_{21} = [1000, -1000]^T m$, $p_{13} = -p_{13} = [0, -2000]^T m$, $p_{23} = -p_{32} = [-1000, -1000]^T m$, respectively. TABLE 1 presents the initial conditions of the group of three UAVs. The acceleration and angular velocity of each member are limited within $a_{max} = \pm 10\text{m/s}^2$ and $w_{max} = \pm 0.15\text{rad/s}$. The constant prediction horizon and constant control update period are set to $T_p = 4\text{s}$ and $\delta = 0.5\text{s}$, respectively. The design of three groups of numerical simulations are given in TABLE 2.

A. EXAMPLE 1 (EVENT-TRIGGERED MECHANISM CONSIDERING E3, E4, E6)

This part presents the simulations of formation control by event-triggered distributed MPC scheme in consideration of predictive distance errors between each UAV E_3, the predictive distance between the formation center and reference trajectory E_4, and the prediction horizon constraint E_6. Fig. 11 shows the ground tracks of each UAV. The solid line represents the traditional MPC method. The dashed line and dotted line represent event-triggered distributed MPC scheme with $\varepsilon_O = 20m$, $\varepsilon_p = 30m$ and $\varepsilon_O = 40m$,

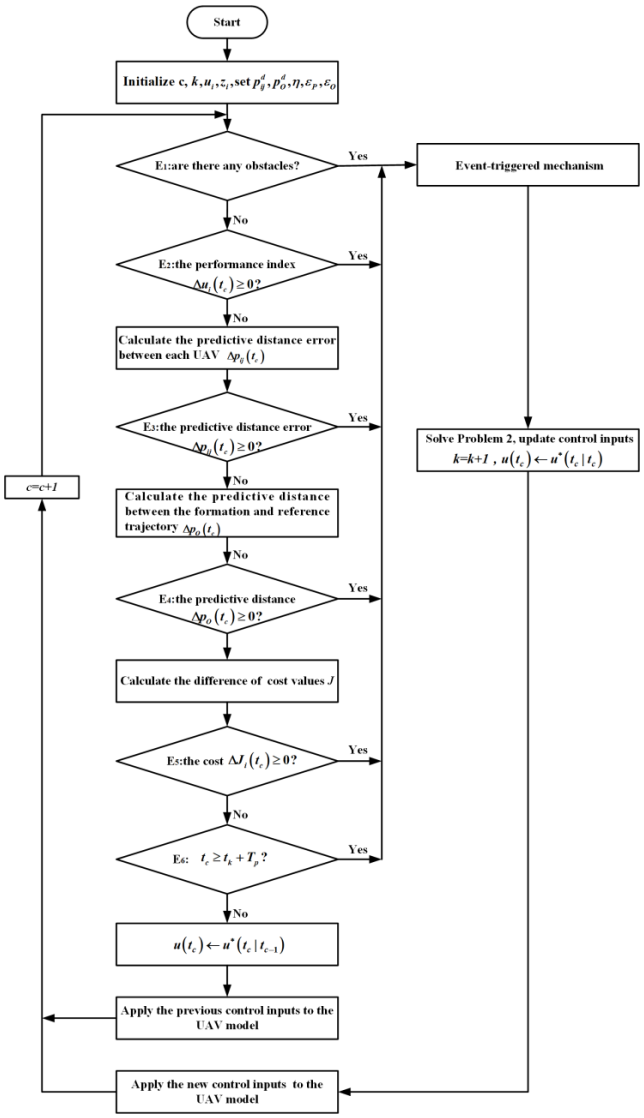

FIGURE 9. The flow chart of the event-triggered mechanism.

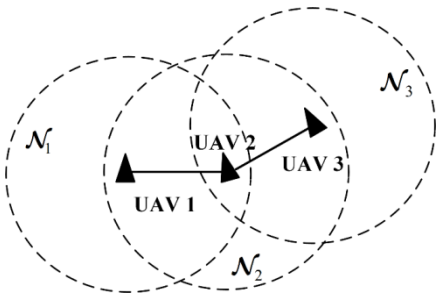

FIGURE 10. Communication topology in the multi-UAV network.

Algorithm 2 Pseudo-Code of the Distributed MPC Scheme Based on the Event-Triggered Mechanism for Each UAV i

1: **// Initialization:** at time t_0
2: Set the parameters: Initialize c,k, p_{ij}^d, p_c^d, η, ε_p, ε_c
3: Initialize the state input: $z_i(t_0)$, $z_{-i}(t_0)$
4: Set $\hat{u}_i(s;t_0) = 0, \hat{u}_{-i}(s;t_0) = 0, s \in [t_0, t_0+T_p]$ and solve **Problem** 2 for UAV i, yielding the optimal predicted control trajectory $u_i^*(s;t_0)$, $s \in [t_0, t_0+T_p]$
5: Apply the first control input $u_i^*(s;t_0)$, $s \in [t_0, t_1)$, the event-triggered instant of UAV i is $t_k, k \in \{1,2,\ldots\}$, $k=1$
6: **// Main loop:** at any time $t_c = t_0 + \delta c, c = \{1,2,\ldots\}$, measure current state $z_i(t_c)$ and transmit $\hat{u}_i(s;t_{c-1})$, $s \in [t_c, t_{c-1}+T_p]$ or $\hat{u}_i(s;t_{c-2})$, $s \in [t_c, t_{c-2}+T_p]$ to its every neighbor
7: If the event-triggered conditions are satisfied, solve **Problem** 2 for UAV i, yielding the optimal predicted control trajectory, $u(t_c) \leftarrow u^*(t_c|t_c)$ and $k = k+1$
8: Else if event-triggered conditions are not satisfied, $u(t_c) \leftarrow u^*(t_c|t_{c-1})$
9: Apply the control input $u(t_c)$, $c = c+1$
10: **// Results**
11: Find the optimal control sequences and generate the complete trajectory
12: Validate the trajectory constraints and terminal conditions

TABLE 1. Initial conditions of three UAVs.

UAVs	x (m)	y (m)	v (m/s)	θ (rad)
UAV 1	-708	-1796	131	1.18
UAV 2	-1848	-53	154	0.38
UAV 3	-1546	1130	138	-0.16

TABLE 2. Examples of numerical simulations.

No.	Examples
1	Event-triggered mechanism considering E_3, E_4 and E_6
2	Event-triggered mechanism considering E_2, E_5 and E_6
3	No-fly zone avoidance considering E_1, E_2, E_4, E_5 and E_6

$\varepsilon_p = 50m$, respectively. The three UAVs are illustrated by red, green and blue colors. It can be seen that the two groups of ground tracks by proposed scheme are similar to ground tracks in the traditional MPC method. In addition, the formation center of the three UAVs is able to track the reference trajectory. Fig. 12 shows the errors between the formation center and reference trajectory, which of the proposed scheme are slightly larger than the traditional MPC method but converge within the desired threshold $\varepsilon_O = 20m$ and $\varepsilon_O = 40m$ before about 18s. Fig. 13 shows the histories of distances between each UAV. Compared to traditional MPC

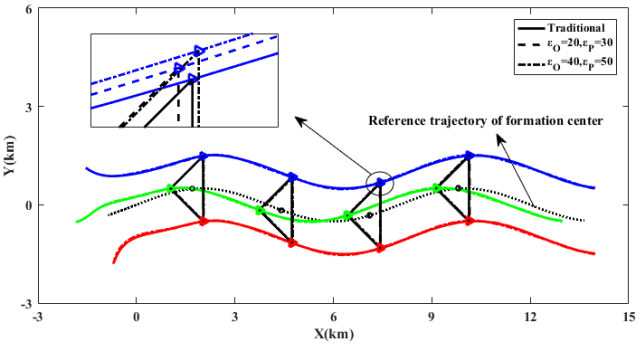

FIGURE 11. Ground tracks of UAVs in Example 1.

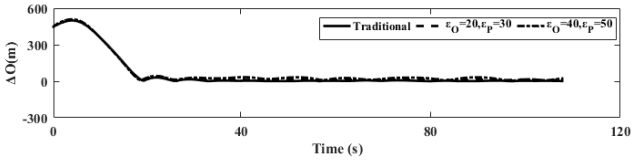

FIGURE 12. Histories of formation center errors in Example 1.

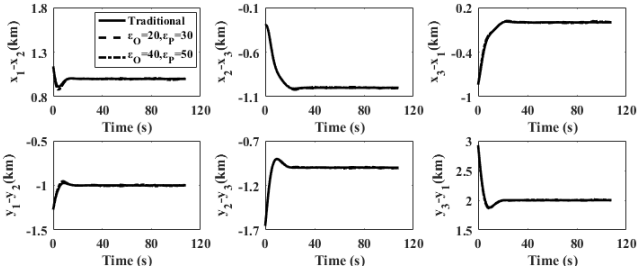

FIGURE 13. Histories of distances between each UAV in Example 1.

method, the errors of distances between each UAV of the proposed scheme are slightly larger but converge within the predetermined threshold $\varepsilon_p = 30m$ and $\varepsilon_p = 50m$ before about 18s.

Fig. 14 shows the event-triggered time instants and cost value for each UAV. Compared to traditional MPC method, it can be seen that the FHOCP do not need to be resolved for each control update period. The cost values of proposed scheme are similar to the traditional MPC method. The total number of time instants for each UAV are shown in the TABLE 3. The largest difference of the number of time instants between the traditional MPC method and proposed scheme with $\varepsilon_O = 20m$, $\varepsilon_p = 30m$ is 91. The largest difference of the number of time instants between the traditional MPC method and proposed scheme with $\varepsilon_O = 40m$, $\varepsilon_p = 50m$ is 122. If the error is acceptable, the number of time instants for proposed scheme are greatly reduced compared to the traditional MPC method. Moreover, the increase of the given thresholds of state errors may result in the increase of average number of time instants when the error is acceptable. Fig. 15 shows the yaw angle and linear velocity as well as control inputs of each UAV. As it can be seen that the control

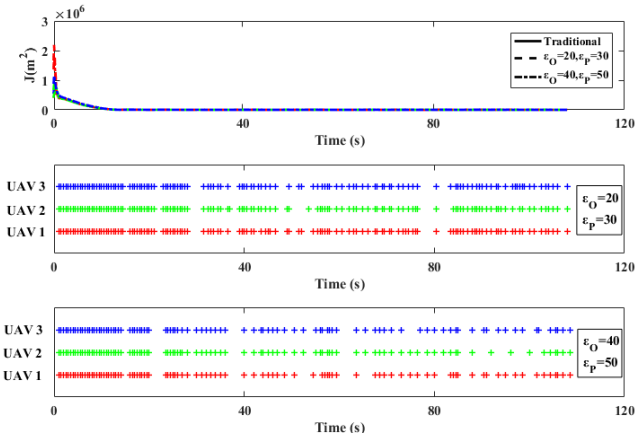

FIGURE 14. The event-triggered time instants in Example 1.

TABLE 3. The total number of time instants for each UAV in Example 1.

UAVs	Traditional	$\varepsilon_O = 20m$, $\varepsilon_p = 30m$	$\varepsilon_O = 40m$, $\varepsilon_p = 50m$
UAV 1	216	130	94
UAV 2	216	126	94
UAV 3	216	125	96

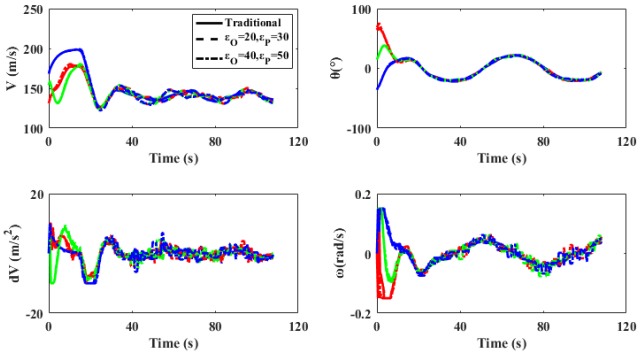

FIGURE 15. Histories of control and state inputs in Example 1.

inputs of each UAV reach saturation at the beginning of the formation, but not exceed the threshold throughout the whole formation control.

B. EXAMPLE 2 (EVENT-TRIGGERED MECHANISM CONSIDERING E2, E5, E6)

This part presents the simulations of formation control by event-triggered distributed MPC scheme in consideration of the saturation level of predictive control inputs E_2, the convergence of predictive cost function E_5, and the prediction horizon constraint E_6. Fig. 16 shows the ground tracks of each UAV. The solid line represents the traditional MPC method. The dashed line and dotted line represent event-triggered distributed MPC scheme with $\Delta k = 1$ and $\Delta k = 3$,

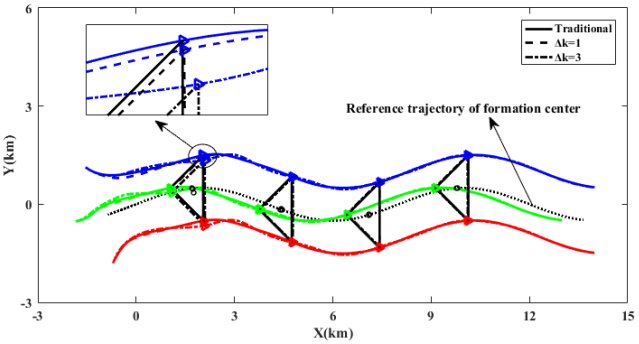

FIGURE 16. Ground tracks of UAVs in Example 2.

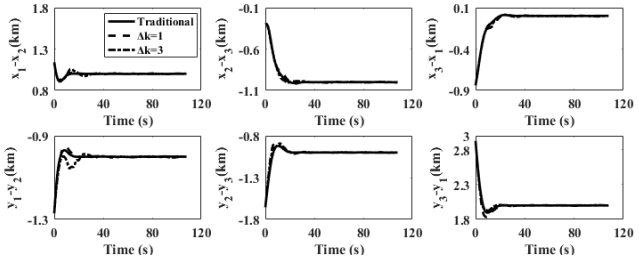

FIGURE 17. Histories of distances between each UAV in Example 2.

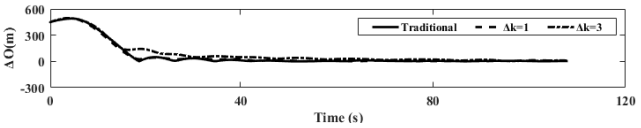

FIGURE 18. Histories of formation center errors in Example 2.

respectively. It can be seen that the two groups of ground tracks by proposed scheme are similar to ground tracks in the traditional MPC method. In addition, the formation center of the three UAVs is able to track the reference trajectory. Fig. 17 shows the histories of distances between each UAV. Compared to traditional MPC method, the errors of distances between each UAV of the proposed scheme are slightly larger but converge within 10m before about 29s. Fig. 18 shows the errors between the formation center and reference trajectory, which of the proposed scheme are slightly larger than the traditional MPC method but converge within 70m before about 23s.

Fig. 19 shows the event-triggered time instants and cost values for each UAV. Compared to traditional MPC method, it can be seen that the computational burden for each UAV is significantly reduced with a smaller number of event-triggered time instants. The cost values of proposed scheme are similar to the traditional MPC method. The total number of time instants for each UAV are shown in the TABLE 4. The largest difference of the number of time instants between the traditional MPC method and proposed scheme with $\Delta k = 1$ is 107. The largest difference between the traditional MPC method and proposed scheme with $\Delta k = 3$ is 132. If the error is acceptable, the number of time instants for proposed

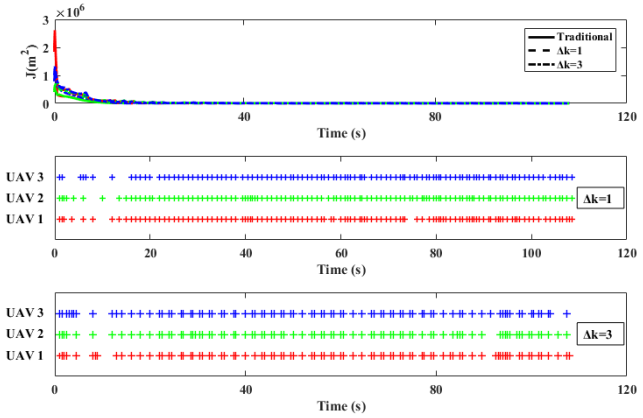

FIGURE 19. The event-triggered time instants in Example 2.

TABLE 4. The total number of time instants for each UAV in Example 2.

UAVs	Traditional	$\Delta k = 1$	$\Delta k = 3$
UAV 1	216	116	88
UAV 2	216	115	84
UAV 3	216	109	87

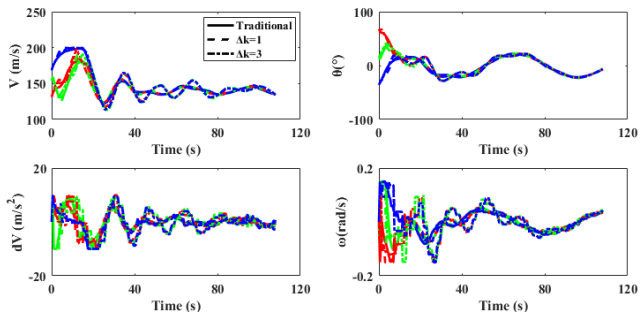

FIGURE 20. Histories of control and state inputs in Example 2.

scheme are greatly reduced compared to the traditional MPC method. Moreover, the increase of the given thresholds of ΔJ may result in the increase of average number of time instants when the error is acceptable. In Example 1, the predictive distance errors between each UAV are larger than the threshold at the beginning of formation flight. The event-triggered conditions are satisfied frequently. However, the predictive cost value is in a declining state at the beginning of the formation flight in Example 2. The event-triggered conditions are satisfied less frequently. Therefore, the event-triggered time instant numbers of proposed scheme are much less at the beginning of formation flight. In addition, the errors of formation are slightly larger before about 40s. Fig. 20 shows the yaw angle and linear velocity as well as control inputs of each UAV. As it can be seen that the control inputs of each UAV reach saturation at the beginning of the formation, but not exceed the threshold throughout the whole formation control.

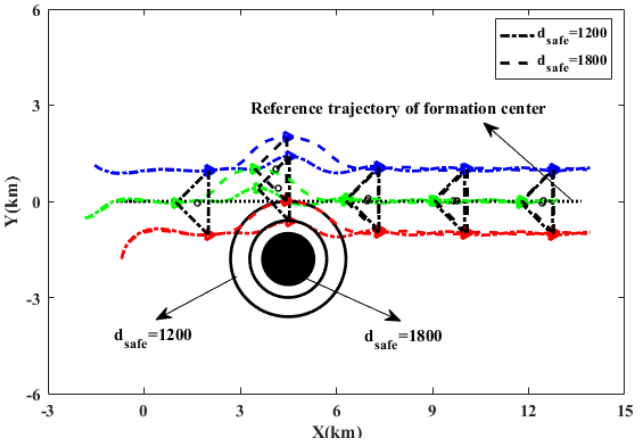

FIGURE 21. Ground tracks of UAVs in Example 3.

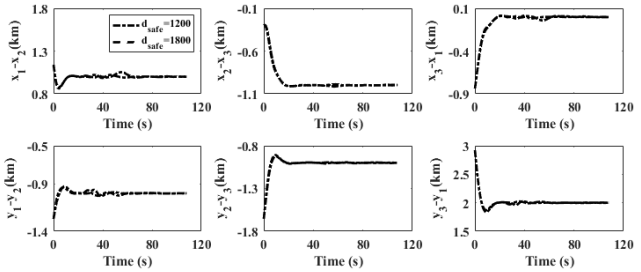

FIGURE 22. Histories of distances between each UAV in Example 3.

C. EXAMPLE 3 (NO-FLY ZONE AVOIDANCE CONSIDERING EVENT-TRIGGERED CONDITIONS E1, E2, E4, E5, E6)

This part presents the simulations of formation control by event-triggered distributed MPC scheme that takes into consideration event-triggered conditions E_1, E_2, E_4, E_5 and E_6. Fig. 21 shows the ground tracks of each UAV. The dashed line and dotted line represent event-triggered distributed MPC scheme with $d_{safe} = 1200$m, $\Delta\varepsilon_p = 30m$, $\eta = 1$, $\Delta k = 3$ and $d_{safe} = 1800$m, $\Delta\varepsilon_p = 30m$, $\eta = 1$, $\Delta k = 3$, respectively. It can be seen that the two groups of ground tracks bypass the no-fly zone. When the event-triggered condition E1 is satisfied for UAV 1, the yaw angle is changed to avoid no-fly zone. At the same time, UAV 2 and UAV 3 keep the formation, but do not track the reference trajectory until the no-fly zone is avoided. The formation center of the three UAVs is able to track the reference trajectory after the no-fly zone avoidance. Fig. 22 presents the histories of distances between each UAV. Although the errors of distances between each UAV are slightly increased when the no-fly zone avoidance, the errors of distances of the proposed scheme converge within the predetermined threshold $\Delta\varepsilon_p = 30m$ before about 17s.

Fig. 23 shows cost values of each UAV for the formation flight and the event-triggered time instants during 25s and 75s. The cost values of the proposed scheme increase during the no-fly zone avoidance. The safe distance is changed from 1200m to 1800m, which leads to a larger cost value. The total number of time instants for each UAV are

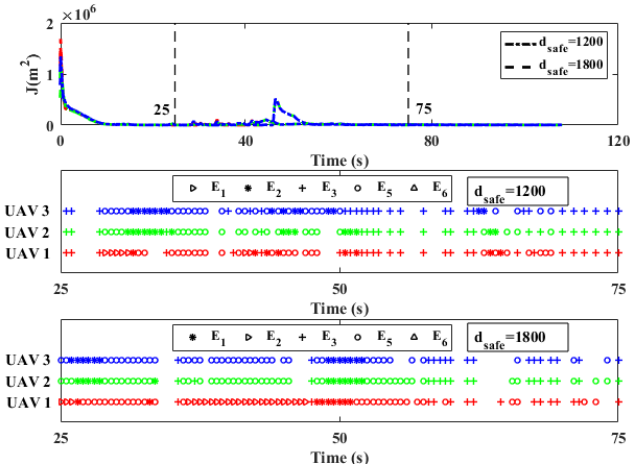

FIGURE 23. The event-triggered time instants in Example 3.

TABLE 5. The total number of time instants for each UAV in Example 3.

UAVs	E_1	E_2	E_3	E_5	E_6	Total numbers (d_{safe}=1200m /d_{safe}=1800m).
UAV 1	7/26	10/11	66/51	57/57	0/0	140/145
UAV 2	0/0	22/19	64/55	55/37	0/0	136/143
UAV 3	0/0	20/19	67/56	55/61	0/0	142/136

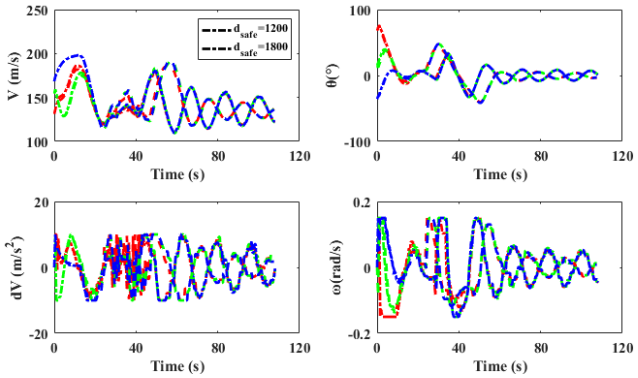

FIGURE 24. Histories of control and state inputs in Example 3.

shown in the TABLE 5. If the error is acceptable, the increase of the safe distance may result in the increase of average number of time instants. Fig. 24 shows the yaw angle and linear velocity as well as control inputs of each UAV. As it can be seen that the control inputs of each UAV reach saturation at the beginning of the formation and when the no-fly zone avoidance, but not exceed the threshold throughout the whole formation control.

D. DISCUSSION

At the beginning of formation flight, the FHOCP in the MPC scheme will be solved frequently, because the predictive distance errors between each UAV are larger than the given threshold and the event-triggered conditions E_3 and E_4 are easily satisfied. When the UAVs keep flying in formation, the distance errors between each UAV become small and the number of event-triggered instants will decrease, which may lead to weak computation burden. However, the cost value typically decreases at the beginning of the formation flight, and therefore, the event-triggered conditions E_5 are hardly satisfied, which causes less numbers of solutions of FHOCP. During no-fly zone avoidance, the event-triggered conditions E_1 is satisfied continuously, and thus, the FHOCP in the MPC scheme will be also continuously solved which increases the computation burden. The saturation level of control inputs is also considered in the design of event-triggered mechanism to improve the control performance. When the predictive control inputs exceed the desired threshold, the event-triggered conditions E_2 is satisfied and the FHOCP will be solved to ensure the overall performance of distributed MPC scheme for UAV formation control. The influence of event-triggered condition E_6 on control performance and computation burden is weak, because the event-triggered condition E_6 is satisfied only when the execution of control input commands is completed during the predicted horizon. In conclusion, the priority and selection of the event-triggered conditions are mainly determined according to different flight missions. The numerical results also show that different event-triggered conditions can improve the performance of the distributed MPC scheme for UAV formation control.

The main idea of the paper is to develop a new solution framework for UAV formation control. The traditional MPC approaches have been demonstrated effective to solve cooperative control of multiple robot and multiple UAVs. However, most MPC schemes for cooperative flight control are designed on the basis of time-triggered mechanism. The control actions are periodically executed even if the systems have achieved desired control performance. The main contribution of this paper is the design of an improved MPC with event-triggered mechanism that can enable the FHOPC to be solved asynchronously. The numerical results show that by the proposed MPC scheme, the computation frequency of FHOCP can be reduced to a certain extent.

V. CONCLUSION

An event-triggered distributed MPC scheme for formation control of multiple UAVs is studied in this paper. A framework of distributed MPC scheme is developed for UAV formation control in which each UAV only shares information with the neighbors. The obtained local FHOCP can be solved by PSO algorithm asynchronously. An event-triggered mechanism is proposed for the distributed MPC scheme considering the predictive state errors and the convergence of cost function, which can reduce the computational burden. The safe-distance-based strategy for no-fly zone avoidance is developed and integrated into the local cost function for UAV formation control. The numerical results show that, the number of solving FHOPC and the computational burdens of multiple UAVs are both effectively reduced when errors

are acceptable. In addition, the increase of the given thresholds or safe distance may result in the increase of average number of time instants. The results also show that a larger safe distance results in the earlier and longer saturation of the control inputs. The paper now lacks an explicit analysis of feasibility and stability of the whole system, and in the future, will focus on systematical theory analysis of the stability condition to ensure feasible solutions of the proposed event-triggered MPC scheme for UAV formation control. The computational complexity is also one of challenging issues to improve the performance of the MPC scheme, and is not mathematically discussed here, which should be studied in the future work.

REFERENCES

[1] J. Chen, Q. Wu, Y. Xu, Y. Zhang, and Y. Yang, "Distributed demand-aware channel-slot selection for multi-UAV networks: A game-theoretic learning approach," *IEEE Access*, vol. 6, pp. 14799–14811, 2018.
[2] S. Zhao *et al.*, "A robust real-time vision system for autonomous cargo transfer by an unmanned helicopter," *IEEE. Trans. Ind. Electron.*, vol. 62, no. 2, pp. 1210–1219, Feb. 2015.
[3] K. Wu, Z. Cai, J. Zhao, and Y. Wang, "Target tracking based on a nonsingular fast terminal sliding mode guidance law by fixed-wing UAV," *Appl. Sci.*, vol. 7, no. 4, p. 333, Mar. 2017.
[4] Q. Zhu, R. Zhou, and J. Zhang, "Connectivity maintenance based on multiple relay UAVs selection scheme in cooperative surveillance," *Appl. Sci.*, vol. 7, no. 1, p. 8, Dec. 2016.
[5] L. He, P. Bai, X. Liang, J. Zhang, and W. Wang, "Feedback formation control of UAV swarm with multiple implicit leaders," *Aerosp. Sci. Technol.*, vol. 72, pp. 327–334, Jan. 2018.
[6] X. Dong, B. Yu, Z. Shi, and Y. Zhong, "Time-varying formation control for unmanned aerial vehicles: Theories and applications," *IEEE Trans. Control Syst. Technol.*, vol. 23, no. 1, pp. 340–348, Jan. 2015.
[7] Q. Luo and H. Duan, "Distributed UAV flocking control based on homing pigeon hierarchical strategies," *Aerosp. Sci. Technol.*, vol. 70, pp. 257–264, Nov. 2017.
[8] A. Karimoddini, H. Lin, B. M. Chen, and H. L. Tong, "Hybrid formation control of the unmanned aerial vehicles," *Mechatronics*, vol. 21, no. 5, pp. 886–898, May 2011.
[9] D. Zhang and H. Duan, "Switching topology approach for UAV formation based on binary-tree network," *J. Franklin Inst.*, to be published, doi: 10.1016/j.jfranklin.2017.11.026.
[10] W. Lin, "Distributed UAV formation control using differential game approach," *Aerosp. Sci. Technol.*, vol. 35, no. 1, pp. 54–62, 2014.
[11] E. Zhao, T. Chao, S. Wang, and M. Yang, "Finite-time formation control for multiple flight vehicles with accurate linearization model," *Aerosp. Sci. Technol.*, vol. 71, pp. 90–98, Dec. 2017.
[12] Z. Chao, S.-L. Zhou, L. Ming, and W. G. Zhang, "UAV formation flight based on nonlinear model predictive control," *Math. Problems Eng.*, 2012, Art. no. 261367, doi: 10.1155/2012/261367.
[13] Z. Peng, B. Li, X. Chen, and J. Wu, "Online route planning for UAV based on model predictive control and particle swarm optimization algorithm," in *Proc. Intell. Control Automat. (WCICA)*, Jul. 2012, pp. 397–401.
[14] A. T. Hafez, A. J. Marasco, S. N. Givigi, M. Iskandarani, S. Yousefi, and C. A. Rabbath, "Solving multi-UAV dynamic encirclement via model predictive control," *IEEE Trans. Control Syst. Technol.*, vol. 23, no. 6, pp. 2251–2265, Nov. 2015.
[15] J. Zhao, S. Zhou, and R. Zhou, "Distributed time-constrained guidance using nonlinear model predictive control," *Nonlinear Dyn.*, vol. 84, no. 3, pp. 1399–1416, May 2016.
[16] J. Zhao and R. Zhou, "Distributed three-dimensional cooperative guidance via receding horizon control," *Chin. J. Aeronaut.*, vol. 29, no. 4, pp. 972–983, Aug. 2016.
[17] D. Groß and O. Stursberg, "A cooperative distributed MPC algorithm with event-based communication and parallel optimization," *IEEE Trans. Control Netw. Syst.*, vol. 3, no. 3, pp. 275–285, Sep. 2016.
[18] Y. Zou, X. Su, and Y. Niu, "Event-triggered distributed predictive control for the cooperation of multi-agent systems," *IET Control Theory Appl.*, vol. 11, no. 1, pp. 10–16, Jan. 2017.
[19] F. D. Brunner, W. P. M. H. Heemels, and F. Allgöwer, "Robust event-triggered MPC with guaranteed asymptotic bound and average sampling rate," *IEEE Trans. Autom. Control*, vol. 62, no. 11, pp. 5694–5709, Nov. 2017.
[20] K. Hashimoto, S. Adachi, and D. V. Dimarogonas, "Distributed aperiodic model predictive control for multi-agent systems," *IET Control. Theory Appl.*, vol. 9, no. 1, pp. 10–20, Jan. 2015.
[21] A. Chakrabarty, S. Zavitsanou, I. F. Doyle, and E. Dassau, "Event-triggered model predictive control for embedded artificial pancreas systems," *IEEE Trans. Biomed. Eng.*, vol. 65, no. 3, pp. 575–586, Mar. 2018.
[22] G. C. S. Cruz and P. M. M. Encarnação, "Obstacle avoidance for unmanned aerial vehicles," *J. Intell. Robotic Syst.*, vol. 65, nos. 1–4, pp. 203–217, 2012.
[23] S. Campbell, W. Naeem, and G. W. Irwin, "A review on improving the autonomy of unmanned surface vehicles through intelligent collision avoidance manoeuvres," *Annu. Rev. Control.*, vol. 36, no. 2, pp. 267–283, Dec. 2012.
[24] M.-C. Fang, S.-M. Wang, M.-C. Wu, and Y.-H. Lin, "Applying the self-tuning fuzzy control with the image detection technique on the obstacle-avoidance for autonomous underwater vehicles," *Ocean Eng.*, vol. 93, pp. 11–24, Jan. 2015.
[25] M. H. Korayem, A. Zehfroosh, H. Tourajizadeh, and S. Manteghi, "Optimal motion planning of non-linear dynamic systems in the presence of obstacles and moving boundaries using SDRE: Application on cable-suspended robot," *Nonlinear Dyn.*, vol. 76, no. 2, pp. 1423–1441, Feb. 2014.
[26] G. Wang, X. Sun, L. Zhang, and C. Lv, "Saturation attack based route planning and threat avoidance algorithm for cruise missiles," *J. Syst. Eng. Electron.*, vol. 22, no. 6, pp. 948–953, Dec. 2011.
[27] W. Yu and W. Chen, "Guidance law with circular no-fly zone constraint," *Nonlinear Dyn.*, vol. 78, no. 3, pp. 1953–1971, Nov. 2014.

ZHIHAO CAI received the Ph.D. degree in guidance, navigation, and control from Beihang University, Beijing, China. He is currently an Associate Professor with the School of Automation Science and Electrical Engineering, Beihang University. His areas of expertise include UAV autonomous navigation, UAV formation flight, V/STOL UAV control, and artificial intelligent control.

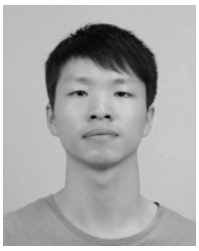

HUI ZHOU is currently pursuing the master's degree in guidance, navigation, and control with the School of Automation Science and Electrical Engineering, Beihang University, Beijing, China. His areas of expertise include flight control, UAV autonomous navigation, and UAV formation control.

JIANG ZHAO received the Ph.D. degree in guidance, navigation, and control from Beihang University, Beijing, China. He is currently a Lecturer with the School of Automation Science and Electrical Engineering, Beihang University. His areas of expertise include flight control and guidance, constrained trajectory optimization, and cooperative control.

KUN WU received the Ph.D. degree in guidance, navigation, and control from Beihang University, Beijing, China. He is currently a Lecturer with the Flying College, Beihang University. His areas of expertise include UAV formation control, UAV cooperative path planning, and UAV autonomous decision.

YINGXUN WANG is currently a Professor in guidance, navigation, and control with the School of Automation Science and Electrical Engineering, Beihang University, Beijing, China. His current works include UAV autonomous flight control and guidance, V/STOL UAV modeling, identification, and control, intelligent navigation, and systems engineering.